

Research on the Influence of Train Speed Change on the EMI of Pantograph-Catenary Arc to Main Navigation Stations

Yutao Tang, Feng Zhu, and Yingying Chen

School of Electrical Engineering
Southwest Jiaotong University, Chengdu, 610031, China
tangyutao@my.swjtu.edu.cn, zhufeng@swjtu.edu.cn, 454621625@qq.com

Abstract — The electromagnetic interference (EMI) of the pantograph-catenary arc (PCA) to the main navigation stations will be affected when the speed of the high-speed train is changed. In order to study the influence of the speed change, we measured and analyzed the electric field intensity of the PCA generated at common and neutral section of power supply line at different train speeds. The frequency range in this study is the frequency of the main navigation stations (108 ~ 336 MHz). Both theoretical and experimental results show that PCA radiation increases with the increase of train speed. Besides, we calculated the maximum train speed without interfering the navigation signal. This work is useful for estimating EMI of the PCA at different train speeds and mitigating the interference to the navigation station near the high-speed railway by proposing corresponding speed limits.

Index Terms — Airport navigation stations, electromagnetic interference, pantograph-catenary arc, speed of high-speed train.

I. INTRODUCTION

Nowadays, it is inevitable for the high-speed train to enter the airport electromagnetic (EM) environmental protection zone to facilitate the transfer of passengers [1]. Therefore, it is necessary to evaluate whether the pantograph-catenary arc (PCA) will interfere with the airport navigation station [2]. However, the influence of the train speed on the EM radiation of the PCA has not been taken into account in the existing evaluation process of potential EM interference (EMI) on the airport navigation stations [3].

Some researchers used the arc simulation model or experimental systems to study the effect of train speed on voltage, current, power, and shape of the PCA [4-6]. In Ref. [7], researchers studied the relationship between train speed and the PCA. However, their data came from the simulation device in the reverberation chamber, which is somewhat different from the actual measurement results of the real train. Our team has done many practical measurements of the PCA and

assessments of the EM environment at airports [8-10]. But the impact of the speed change on PCA radiation was not considered in previous studies.

As an extension of previous works, firstly, the characteristics of the PCA generated at two typical positions of the power supply line—common and neutral sections are analyzed. Secondly, taking one high-speed railway as the test object, the electric field intensity of the PCA is measured at different train speeds. Thirdly, the linear regression method is used to process and analyze the measurement data. Then, the amplitude-frequency characteristic curves of the PCA at different speeds are fitted. It should be noted that the frequency ranges are the frequency of main airport navigation stations: Omnidirectional Beacon Station (OBS) (108 ~ 117.975 MHz), Very-High-Frequency Communication System (VHFCS) (118 ~ 136.975 MHz), and Glide Beacon Station (GBS) (328.6 ~ 335.4 MHz). Finally, the maximum train speed that can guarantee the airport navigation signals to be normal is calculated. The results of this paper can provide the basis for perfecting the existing assessment of the airport EM environment.

II. ANALYSIS OF THE EFFECT OF TRAIN SPEED ON THE PCA

A. Characteristics of the PCA at the common sections

The high-speed train gets electricity power by connecting its pantographs to the power supply line. The reason for generating the PCA at the common sections is that there are some fixed hard-points on the power supply line. When the train passes through the hard-points, the pantograph and the line will be separated for a short time. Besides, the diameter and the convective power (P_k) of the PCA will change with the train speed. Moreover, P_k includes the convective power generated by the transverse arc blowing (P_{kT}) and by the longitudinal arc blowing (P_{kL}) [11]. The distance between the pantograph and the power supply line (r_{com}) is short. Thus, only P_{kT} exists because the PCA is almost vertical as shown in Fig. 1.

P_{kT} of the PCA can be obtained by [12]:

$$P_{KT}' = 0.1464d(v+36)^{1.5}, \quad (1)$$

where P_{KT}' is P_{KT} per unit length of the PCA, v is the train speed, which unit is km/h.

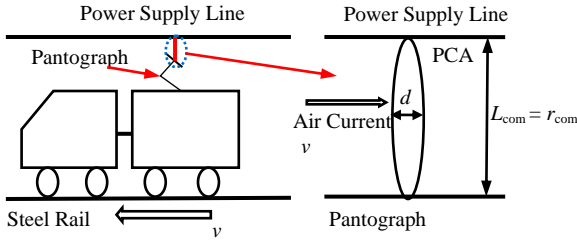


Fig. 1. Diagram of the PCA generated at the common section.

The diameter of the arc (d) is reduced by the transverse airflow and d can be calculated by [13, 14]:

$$d = 1.5369 \sqrt{\frac{I/\sqrt{2}}{v+36}}, \quad (2)$$

where I is the maximum value of the PCA current.

P_{KT}' can be calculated by Eq. (1) and Eq. (2):

$$P_{KT}' = 0.1892\sqrt{I}(v+36). \quad (3)$$

The length of the PCA at the common section (L_{com}) is about 10 mm, which is the same as r_{com} . The convective power of the PCA at common sections ($P_{k(com)}$) can be obtained by Eq. (3):

$$P_{k(com)} = P_{KT} = P_{KT}' \cdot L_{com} = 1.892\sqrt{I}(v+36), \quad (4)$$

where $P_{k(com)}$ and radiation power ($P_{s(com)}$) of the PCA account for approximately 80% and 20% of the total dissipative power ($P_{loss(com)}$), respectively. So $P_{loss(com)}$ and $P_{s(com)}$ of the PCA at the common sections are:

$$P_{loss(com)} = \frac{P_{k(com)}}{80\%}, \quad (5)$$

and

$$P_{s(com)} = 20\% P_{loss(com)} = 0.473\sqrt{I}(v+36). \quad (6)$$

B. Characteristics of the PCA at the neutral sections

The reason for generating the PCA at the neutral sections is that the pantograph need to be separated from the original power supply line and enter into the neutral line to realize the voltage phase conversion. The distance between the pantograph and the power supply line (r_{neu}) is long. Thus, both P_{KT} and P_{KL} exist because the PCA has an angle with the horizontal plane as shown in Fig. 2. At this time, the length of PCA will be elongated because of the multiple external forces, and its stress diagram is shown in Fig. 3. Where F_{wind} is the wind load force; F_{float} is the thermal buoyancy force; F_m is the magnetic force (the direction is related to the direction of magnetic field).

If the PCA keeps uniform motion in a short time and the mass of it is negligible at high temperature.

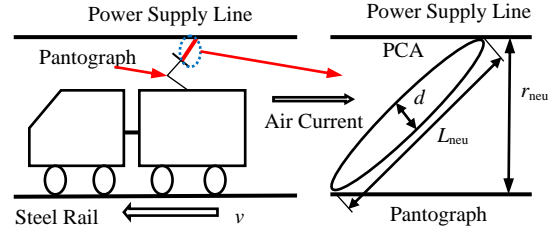


Fig. 2. Diagram of the PCA generated at the neutral section.

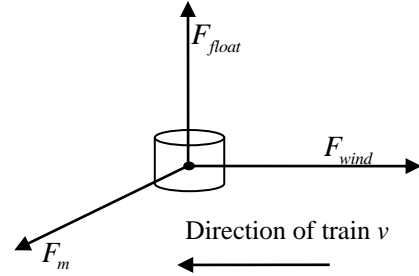


Fig. 3. Force diagram of the PCA generated at the neutral section.

The resultant force on the PCA is:

$$F_{wind} + F_{float} + F_m = 0. \quad (7)$$

If r_{neu} is 15 mm, the direction of the initial PCA is vertical and the initial length is equal to r_{neu} . The diagram of the length of the PCA at the neutral section (L_{neu}) variation with external force can be obtained by simulation calculation, as shown in Fig. 4.

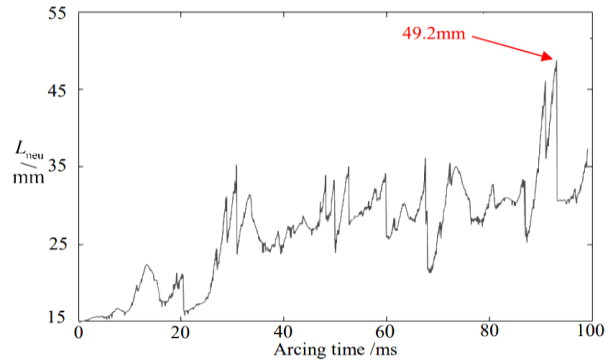


Fig. 4. Diagram of the L_{neu} change caused by the external force.

The simulation results show that the PCA increases with the arcing time until it reaches the critical length

and extinguished. The maximum of L_{neu} is about 49.2 mm. Therefore, the L_{neu} is about 3.28 times of the r_{neu} .

Based on the simulation and measurement data from [15], r_{neu} can be fitted by:

$$r_{neu} = 4.571 \times 10^{-5} v^2 + 0.238v - 1.411. \quad (8)$$

So,

$$L_{neu} = 3.28r_{neu} = 1.5 \times 10^{-4} v^2 + 0.78v - 4.628. \quad (9)$$

P_{kl} of the PCA at the neutral section is [16]

$$P_{kl}' = 0.2182d^2 v \int_{T_0}^{T_C} C dT, \quad (10)$$

where P_{kl}' is P_{kl} per unit length of the PCA, which is produced by air heating from temperature T_0 to the average temperature of the arc T_C . T_0 and T_C are 4000 K and 9500, respectively. C is the heat capacity coefficient of air and C is [17]:

$$C \approx \frac{0.41}{T}. \quad (11)$$

P_{kl}' can be derived by Eq. (2) and Eqs. (9) ~ (11):

$$P_{kl}' = 0.13\sqrt{I} \frac{v}{v+36}. \quad (12)$$

The convective power of the PCA at neutral sections ($P_{k(neu)}$) can be obtained by Eq. (3) and Eq. (12):

$$P_{k(neu)} = \sqrt{I} [0.1892(v+36) + 0.13 \frac{v}{v+36}] \cdot (1.5 \times 10^{-4} v^2 + 0.78v - 4.628). \quad (13)$$

It is similar to the above, $P_{loss(neu)}$ and $P_{s(neu)}$ of the PCA at neutral sections are:

$$P_{loss(neu)} = \frac{P_{k(neu)}}{80\%}, \quad (14)$$

and

$$P_{s(neu)} = 0.25\sqrt{I} [0.1892(v+36) + 0.13 \frac{v}{v+36}] \cdot (1.5 \times 10^{-4} v^2 + 0.78v - 4.628). \quad (15)$$

C. The E values of the PCA at the common/neutral sections

The values of E at different distances from the PCA are unequal. According to Eq. (6) and Eq. (15), E at 10 m away from the PCA at the common or neutral sections ($E_{10(com/neu)}$) can be derived by:

$$E_{10(com/neu)} = \sqrt{\frac{P_{s(com/neu)}}{4\pi \cdot 10^2}} \cdot 120\pi. \quad (16)$$

The unit of $E_{10(com/neu)}$ is V/m, which can be converted to dB μ V/m by:

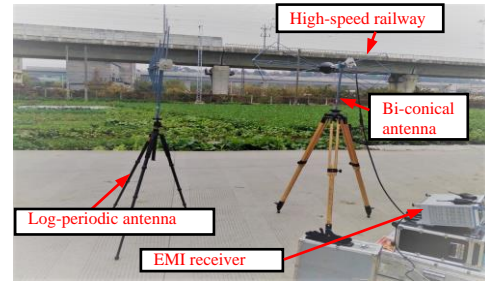
$$E_{10(com/neu)} = 20 \log_{10} (\sqrt{0.3P_{s(com/neu)}}) + 120. \quad (17)$$

According to the above analysis, the train speed affects the electric field intensity of the PCA by affecting the radiation power of it. Besides, the faster the train speed, the stronger the electric field of the PCA.

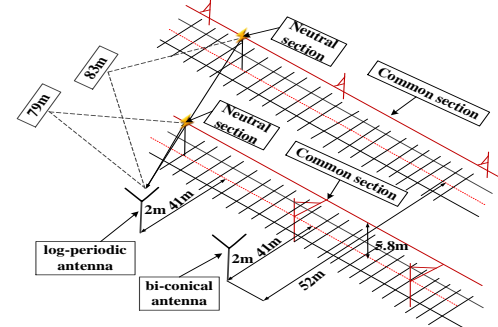
III. PRACTICAL MEASUREMENTS

One high-speed railway (the maximum speed is 250 km/h) in the Sichuan Province of China is taken as the measurement object in this paper. This railway is divided into two parallel tracks for round trips. The PCA usually occurs at the common and neutral sections of the power supply line. For the former, the measurement distance is the linear distance from the antenna to the railroad, and for the latter, it is the distance between the antenna and the neutral sections. Figure 5 shows the scene of the practical measurement (a) and the specific layout (b).

The linear distances from the antenna to the two parallel tracks are 41 m and 52 m. Besides, the distances from the antenna to the neutral sections are 79 m and 83 m, respectively. The height of the antenna is 2 m.



(a) Diagram of the status of the practical measurement



(b) Layout diagram of the measurement

Fig. 5. The situation of the practical measurement.

According to the standards [4, 18], the polarization modes of antennas are horizontal Bi-conical for OBS, perpendicular Bi-conical for VHFCS, and horizontal Log-periodic for GBS. Besides, the resolution bandwidth is 120 KHz and the measurement time is 50 ms. In this paper, the following typical frequency points of the airport navigation stations are selected:

- 1) 108 MHz, 109.7 MHz, 110 MHz, and 115 MHz in the frequency range of OBS.
- 2) 119 MHz, 126.48 MHz, 128 MHz, and 135 MHz

in the frequency range of VHFCS.

3) 329.3 MHz, 330.5 MHz, and 332 MHz in the frequency range of GBS.

The maximum value of E is used to analyze the most serious radiation. For comparison purposes, the results are converted to values at 10 m equivalent distance by:

$$E_{10} = E_D + n \times 20 \log_{10}(D/10), \quad (18)$$

where E_{10} and E_D are E at the distance of 10 m and D m from the PCA; n is the coefficient related to frequency. When the frequencies are 108 MHz and 109.7 MHz, n is 1.2, and the others are 1. Due to the large amount of measurement data, this paper does not list the complete data. Table 1 lists the data obtained after the abnormal measurement data were excluded by *Grubbs* method [19] and replaced by retest.

Table 1: Part of testing data ($v = 250$ km/h)

Frequency (MHz)	E (dB μ V/m)		Distance (m)		E_{10} (dB μ V/m)	
	Common Section	Neutral Section	Common Section	Neutral Section	Common Section	Neutral Section
108	40.78	52.07	41	79	55.49	73.62
109.7	38.2	51.45	52	83	55.38	73.51
110	43.11	55.54	41	79	55.37	73.49
115	40.75	54.80	52	83	55.07	73.18
119	40.53	54.99	52	79	54.85	72.94
126.48	42.2	54.14	41	83	54.46	72.52
128	42.12	54.48	41	79	54.38	72.43
135	39.7	53.68	52	83	54.02	72.06
329.3	35.93	47.49	41	83	48.19	65.87
330.5	33.84	47.89	52	79	48.16	65.84
332	35.88	47.86	41	79	48.14	65.81

IV. PROCESSING AND ANALYSIS OF MEASUREMENT DATA

A. Amplitude-frequency curves of E of the PCA

To find out the relationship between frequency (f) and E_{10} , the correlation between the two variables is determined by [19]:

$$r = \frac{\sum_{i=1}^N [\log_{10}(f_i) \times E_{10i}] - N \times \overline{\log_{10}(f)} \times \overline{E_{10}}}{\sqrt{(\sum_{i=1}^N [\log_{10}(f_i)]^2 - N \times \overline{\log_{10}(f)}^2) \times (\sum_{i=1}^N E_{10i}^2 - N \times \overline{E_{10}}^2)}}, \quad (19)$$

where i is the ordinal number of the samples; N is the total number of the samples; r is the correlation coefficient between f and E_{10} . The parameters marked with a hat denote the mean. $N=11$ and $r \approx -0.99$ are calculated by Table 1 and Eq. (19). The negative correlation between f and E_{10} is very strong because of $r \in [-1, -0.75]$. Therefore, the two variables satisfy the linear correlation. The linear regression equation between f and E_{10} can be expressed as:

$$E_{10} = a \log_{10}(f) + b, \quad (20)$$

where a is the regression coefficient, and b is the intercept. They are calculated by:

$$\begin{cases} a = \frac{\sum_{i=1}^N [\log_{10}(f_i) \times E_{10i}] - N \times \overline{\log_{10}(f)} \times \overline{E_{10}}}{\sum_{i=1}^N [\log_{10}(f_i)]^2 - N \times \overline{\log_{10}(f)}^2} \\ b = \overline{E_{10}} - a \times \overline{\log_{10}(f)} \end{cases} \quad (21)$$

For OBS, VHFCS, and GBS (108 ~ 336 MHz), when the train passes through the common section at a speed of roughly 250 km/h, $a \approx -15.08$ and $b \approx 86.15$ can be calculated by Eq. (21). Thus, the relationship between f and E_{10} is derived by:

$$E_{10} = -15.08 \log_{10}(f) + 86.15. \quad (22)$$

Similarly, the curves of f and E_{10} at different speeds can be obtained, and the relevant parameters are shown in Table 2.

Table 2: The parameters of relation curves

Frequency (MHz)	Site	Speed (km/h)	a	b
108 ~ 336 (OBS, VHFCS, and GBS)	Common Section	80	-12.59	73.19
		110	-13.59	76.39
		130	-14.05	78.46
		175	-14.78	82.15
		250	-15.08	86.15
	Neutral Section	110	-15.05	97.44
		130	-15.15	98.44
		180	-15.32	100.54
		200	-15.50	102.74
		250	-16.00	106.15

B. EMI limit of navigation signals

This high-speed train will cross the extension line of an airport runway. The locations and distances are shown in Fig. 6, where X is the intersection of the railway and extension line of airport runway; h is the altitude of the aircraft from X; d_{s1} , d_{s2} , and d_{s3} are the distances from OBS, VHFCS, and GBS to the airplane.

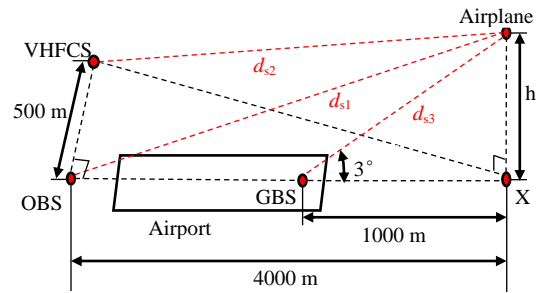


Fig. 6. The location and distance of the navigation equipment, aircraft, and intersection.

The signal strength (E_s) of the navigation stations is specified by [20]:

$$E_s = 134.77 + 10 \log_{10} P + G - 20 \log_{10} d_s, \quad (23)$$

where P and G are the transmission power and the antenna gain of the navigational equipment; d_s is the distance from the navigational equipment to the aircraft. The relevant parameters of the navigational equipment in this paper are shown in Table 3, where R is the margin to ensure normal navigation signals. At the same frequency, the signal strength (E_s) of the navigational stations should be at least R dB more than the E value of EMI, namely, $E_s - E \geq R$.

Table 3: Relevant parameters of navigation equipment

Name	P (W)	G (dB)	d_s (m)	R (dB)
OBS	50.0	2	$d_{s1}=4000.3$	20
VHFCS	20	5	$d_{s2}=1001.4$	
GBS	9.5	14.3	$d_{s3}=4031.5$	

According to Eq. (18), Eq. (23), and Table 3, the maximum limits of EMI at the distance of 10 m ($E_{10(Limit)}$) can be calculated by:

$$E_{10(Limit)} = 94.77 + 10 \log_{10} P + G + 20 \log_{10} \frac{d_n}{d_s}, \quad (24)$$

where d_n is the distance from the PCA to the airplane.

Based on Fig. 6, Table 3, and Eq. (24), $E_{10(Limit)}$ of OBS, VHFCS, and GBS are 71.93 dB μ V/m, 70.88 dB μ V/m, and 89.05 dB μ V/m, respectively.

According to the above results, the influences of the train speed on E_{10} of the PCA in the frequency

range of OBS, VHFCS, and GBS are shown in Fig. 7 and Fig. 8.

As shown in Fig. 7 and Fig. 8, E_{10} of the PCA at the neutral sections is approximately 18 dB higher than that at the common sections. Besides, E_{10} does not exceed $E_{10(Limit)}$ when the train passes through the common sections. However, for neutral sections, E_{10} in the frequency range of OBS and VHFCS will higher than $E_{10(Limit)}$ if the train exceeds a certain speed. Therefore, the X point in Fig. 6 is a sensitive position for OBS and VHFCS.

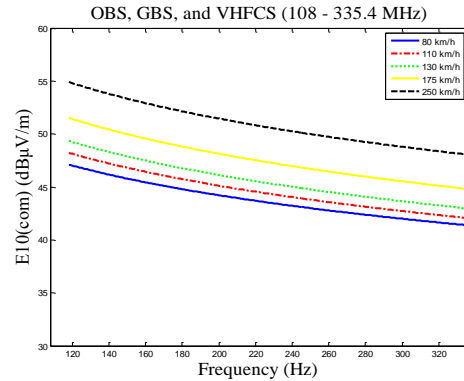


Fig. 7. Diagram of the relationship between the speed and E_{10} at the common sections.

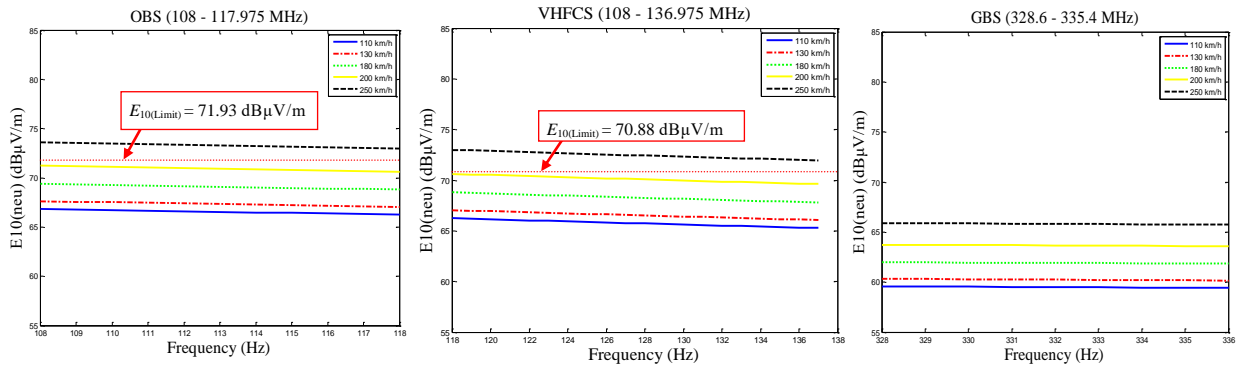


Fig. 8. Diagram of the relationship between the speed and E_{10} at the neutral sections.

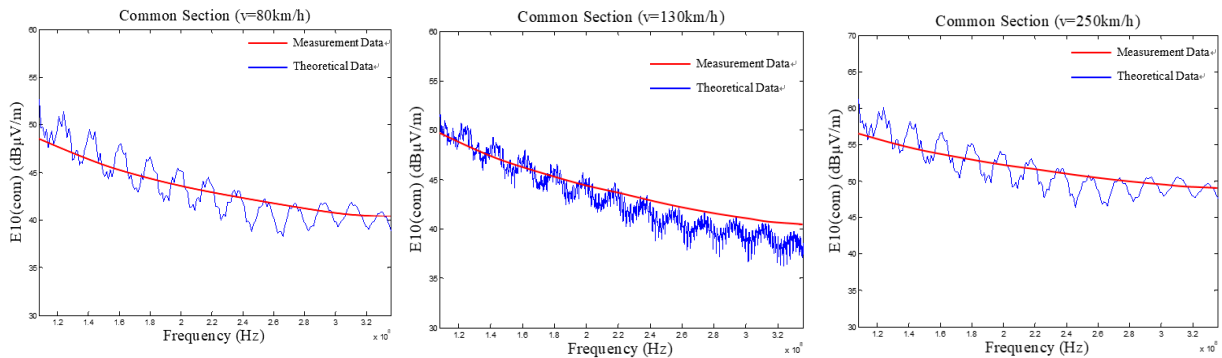


Fig. 9. Comparison of E_{10} of measurement and theoretical results at the common sections.

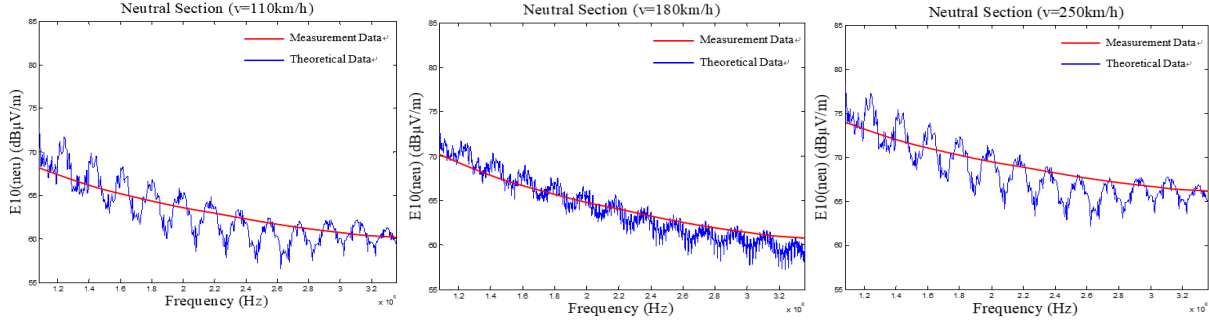


Fig. 10. Comparison of E_{10} of measurement and theoretical results at the neutral sections.

V. CALCULATION OF THE LIMITS OF TRAIN SPEED

The $E_{10(\text{com})}$ values of the train passing through the common sections at a speed of 80 km/h, 130 km/h, and 250 km/h can be calculated by using Eq. (6) and Eq. (17). Its amplitude-frequency relation at 108 ~ 336 MHz can be obtained by Fast Fourier Transform (FFT). The results compared with the measurement data of Fig. 7 are shown in Fig. 9. Similarly, $E_{10(\text{neu})}$ of the train passing through the neutral sections at a speed of 110 km/h, 180 km/h, and 250 km/h are shown in Fig. 10. The average errors of E_{10} are shown in Table 4, which the error is within 10%. It is reasonable because of the error of practical measurements.

Table 4: The E_{10} Error between measurement and theoretical data

Frequency (MHz)	Site	Speed (km/h)	Average Error
108 ~ 336 (OBS, VHFCS, and GBS)	Common Section	80	6.52%
		130	6.96%
		250	4.84%
	Neutral Section	110	8.37%
		180	7.87%
		250	6.65%

As can be seen from the theoretical analysis, the radiated power of the PCA increases with the train speed, which is the main reason for E of the PCA increases with the speed. The maximum train speeds without affecting the signals of the OBS and VHFCS are calculated by Eq. (6), Eq. (15), and Eq. (17). As shown in Fig. 11, E_{10} in the frequency ranges of OBS and VHFCS exceed $E_{10(\text{Limit})}$ (71.93 dB μ V/m and 70.88 dB μ V/m) when the train speed beyond 225 km/h and 215 km/h, respectively.

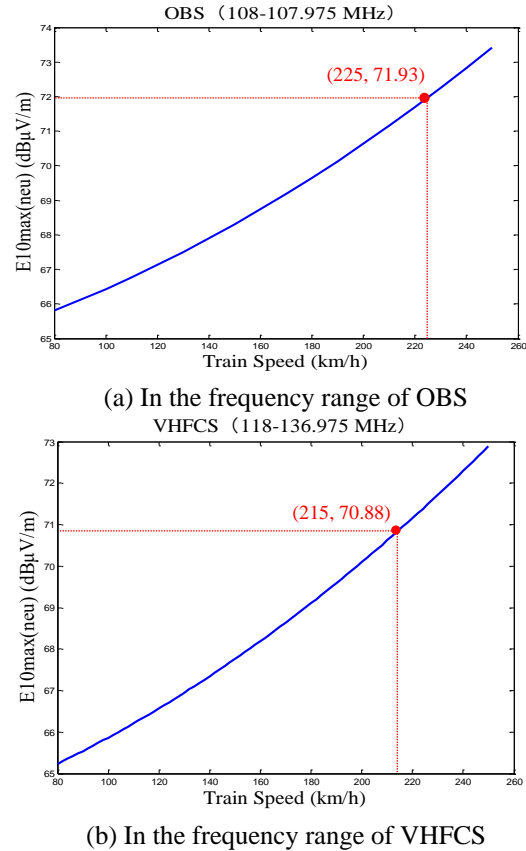


Fig. 11. The curve of the relationship between v and E_{10} maximum at the neutral sections.

VI. CONCLUSION

The influence of the train speed on the electric field intensity (E) of the PCA in the frequency ranges of OBS, VHFCS, and GBS is studied. The conclusions are as follows:

1) If both the speed and the frequency are the same, E at the neutral sections is nearly 18 dB higher than that

at the common sections. Namely, the PCA at the common sections tends to cause less interference.

2) The E values will increase with the train speed at the same frequency range, but it will decrease at higher frequencies. In other words, high-frequency navigation stations (like GBS) are immune to the EMI generated by the PCA.

3) In order to avoid the interference of the PCA on the navigation stations, the neutral sections should not be designed in sensitive positions (like X in Fig. 6) in railway design. If it is inevitable, the train should slow down (not exceeding 215 km/h) when it passes through the sensitive positions.

4) The main reason that the train speed affects E is that the speed can cause the change of the PCA length and further impact the radiation power of the PCA.

To sum up, the speed of high-speed trains can affect the EM radiation of the PCA. Defining appropriate speed limits can alleviate the EMI caused by the PCA to the nearby navigation stations.

ACKNOWLEDGMENT

The authors would like to thank the editors and anonymous reviewers for their insightful comments and thank Ling Zhang for the help in English grammar. This paper is supported by the National Key R&D Program of China (No. 2018YFC0809500).

REFERENCES

- [1] X. Li, F. Zhu, H. Lu, R. Qiu, and Y. Tang, "Longitudinal propagation characteristic of pantograph arcing electromagnetic emission with high-speed train passing the articulated neutral section," *IEEE Trans. Electromagn. Compat.*, vol. 61, no. 2, pp. 319-326, June 2018.
- [2] H. Lu, F. Zhu, Q. Liu, X. Li, Y. Tang, and R. Qiu, "Suppression of cable overvoltage in a high-speed electric multiple units system," *IEEE Trans. Electromagn. Compat.*, vol. 61, no. 2, pp. 361-371, June 2018.
- [3] *Electromagnetic Environment Requirements for Aeronautical Radio Navigation Stations*, GB/T 6364, 2013 (in Chinese).
- [4] W. Wei, T. Zhang, G. Gao, and G. Wu, "Influences of pantograph-catenary arc on electrical characteristics of a traction drive system," *High Voltage Eng.*, vol. 44, no. 5, pp. 1589-1597, May 2018. (In Chinese).
- [5] A. Dong, G. Wu, G. Gao, L. Zhou, and W. Wang, "Simulation system of pantograph arcing," *Electric Power Equipment-Switching Technology 2011 1st Int. Conf. on IEEE*, pp. 637-641, Oct. 2011.
- [6] Y. Wang, Z. Liu, X. Mu, K. Huang, and H. Wang, "An extended Habedank's equation-based EMTP model of pantograph arcing considering pantograph-catenary interactions and train speeds," *IEEE Trans. on Power Del.*, vol. 31, no. 3, pp. 1186-1194, Jan. 2016.
- [7] E. Karadimou and R. Armstrong, "Test of rolling stock electromagnetic compatibility for cross-domain interoperability," *IET Intelligent Transport Systems*, vol. 10, no. 1, pp. 10-16, Feb. 2016.
- [8] F. Zhu, Y. Tang, and C. Gao, "Mechanism and suppression of electromagnetic interference of pantograph-catenary arc to speed sensor of CRH380BL electric multiple unit," *China Railway Science*, vol. 37, no. 6, pp. 69-74, Nov. 2016. (In Chinese).
- [9] Y. Tang and F. Zhu, "Measurement and suppression of electromagnetic interference to speed sensor of CRH380BL electric multiple unit," *2017 International Applied Computational Electromagnetics Society Symposium*, Sept. 2017.
- [10] Y. Tang, F. Zhu, H. Lu, and X. Li, "Analysis and suppression of EMI for traction control unit speed sensors of CRH380BL electric multiple unit," *Applied Computational Electromagnetics Society Journal*, vol. 33, no. 5, pp. 553-560, May 2018.
- [11] X. Chen, B. Cao, Y. Liu, G. Gao, and G. Wu, "Dynamic model of pantograph-catenary arc of train in high speed airflow field," *High Voltage Eng.*, vol. 24, no. 11, pp. 3593-3600, Nov. 2016. (In Chinese).
- [12] X. Yan, W. Chen, and Z. Li, "Simulation for self-extinction behavior of secondary arc in transmission lines," *High Voltage Eng.*, vol. 38, no. 9, pp. 2150-2156, 2012. (In Chinese).
- [13] Y. Liu, G. Chang, and H. Huang, "Mayr's equation-based model for pantograph arc of high-speed railway traction system," *IEEE Trans. on Power Del.*, vol. 25, no. 3, pp. 2025-2027, Aug. 2010.
- [14] H. Zhou, Z. Liu, Y. Cheng, and K. Huang, "Extended black-box model of pantograph arcing considering varying pantograph detachment distance," *2017 IEEE Transportation Electrification Conference and Expo, Asia-Pacific (ITEC Asia-Pacific)*, Harbin, pp. 1-6, 2017.
- [15] Y. Wu, "Research on dynamic performance and active control strategy of high speed pantograph-catenary systems," *Ph.D. dissertation, Dept. Elect. Eng., Beijing Jiaotong Univ.*, Beijing, China, 2011. (In Chinese).
- [16] S. Midya, D. Bormann, T. Schutte, and R. Thottappillil, "Pantograph arcing in electrified railways—Mechanism and influence of various parameters—Part II: With AC traction power supply," *IEEE Trans. on Power Del.*, vol. 24, no. 4, pp. 1940-1950, Sep. 2009.
- [17] S. Li, X. Jin, and H. Bi, "Numerical calculation on very fast transient overvoltage of UHV gas insulated substation by variable gap arc model,"

High Voltage Eng., vol. 41, no. 4, pp. 1306-1312, 2015. (In Chinese).

- [18] *Railway Applications-Electromagnetic Compatibility-Part 2: Emission of the Whole Railway System to the Outside World*, IEC Standard 62236-2, 2018.
- [19] C. Zhang, X. Cai, and Z. Jiang, "Characteristics and measurement of interference sources in electrified railway," *Journal of Beijing Jiaotong Univ.*, no. 2, pp. 13-29, July 1980. (In Chinese).
- [20] J. Gou, F. Zhu, J. Zou, J. Ye, H. Li, and Y. Wang, "Research on EMI of instrument landing system on aircraft caused by pantograph arc," *Journal of the China Railway Society*, vol. 40, no. 7, pp. 61-66, July 2018. (In Chinese).



Yutao Tang was born in Sichuan Province, China, in 1991. She received the B.S. degree in Automation from Southwest Science and Technology University, Mianyang, China, in 2013, and is currently working toward the Ph.D. degree in Electrical Engineering at Southwest Jiaotong University, Chengdu, China.

Her research interests include electromagnetic environment test and evaluation, and electromagnetic compatibility analysis and design.



Feng Zhu was born in Anhui Province, China, in 1963. He received a B.S. degree in Physics from Huaibei Normal University, Huaibei, China, in 1984, an M.S. degree in Physics from Sichuan University, Chengdu, China, in 1987, and the Ph.D. degree in Electromagnetic Theory and Microwave Techniques from Southwest Jiaotong University, Chengdu, in 1997.

He is currently a Professor in the Department of Electrical Engineering, Southwest Jiaotong University. His research interests include electromagnetic environment test and evaluation, electromagnetic compatibility, and numerical electromagnetic methods.



Yingying Chen was born in Shanxi Province, China, in 1996. She received a B.S. degree in Electrical Engineering and Automation from Taiyuan University of Science and Technology in China, in 2018. She is currently pursuing a master's degree in Electrical Engineering at Southwest Jiaotong University, Chengdu, China.

Her research interests include electromagnetic environment testing and evaluation, as well as electromagnetic compatibility analysis and design.